HHS Public Access

Author manuscript

J Biol Methods. Author manuscript; available in PMC 2015 October 23.

Published in final edited form as:

J Biol Methods. 2015 ; 2(3): . doi:10.14440/jbm.2015.77.

Deciphering hepatocellular responses to metabolic and oncogenic stress

Kathrina L. Marcelo[1], **Fumin Lin**[1], **Kimal Rajapakshe**[1], **Adam Dean**[1], **Naomi Gonzales**[1], **Cristian Coarfa**[1], **Anthony R. Means**[1,2], **Lauren C. Goldie**[3,4,5,†], and **Brian York**[1,2,†,*]

[1]Department of Molecular and Cellular Biology, Baylor College of Medicine, Houston, TX, USA

[2]Dan L. Duncan Cancer Center, Baylor College of Medicine, Houston, TX, USA

[3]Department of Pediatrics, Baylor College of Medicine, Houston, TX, USA

[4]Center for Cell and Gene Therapy, Baylor College of Medicine, Houston, TX, USA

[5]USDA/ARS Children's Nutrition Research Center at Baylor College of Medicine, Houston, TX, USA

Abstract

Each cell type responds uniquely to stress and fractionally contributes to global and tissue-specific stress responses. Hepatocytes, liver macrophages (MΦ), and sinusoidal endothelial cells (SEC) play functionally important and interdependent roles in adaptive processes such as obesity and tumor growth. Although these cell types demonstrate significant phenotypic and functional heterogeneity, their distinctions enabling disease-specific responses remain understudied. We developed a strategy for the simultaneous isolation and quantification of these liver cell types based on antigenic cell surface marker expression. To demonstrate the utility and applicability of this technique, we quantified liver cell-specific responses to high-fat diet (HFD) or diethylnitrosamine (DEN), a liver-specific carcinogen, and found that while there was only a marginal increase in hepatocyte number, MΦ and SEC populations were quantitatively increased. Global gene expression profiling of hepatocytes, MΦ and SEC identified characteristic gene signatures that define each cell type in their distinct physiological or pathological states. Integration of hepatic gene signatures with available human obesity and liver cancer microarray data provides further insight into the cell-specific responses to metabolic or oncogenic stress. Our data reveal unique gene expression patterns that serve as molecular “fingerprints” for the cell-centric responses to pathologic stimuli in the distinct microenvironment of the liver. The technical advance highlighted in this study provides an essential resource for assessing hepatic cell-specific contributions to metabolic and oncogenic stress, information that could unveil previously unappreciated molecular mechanisms for the cellular crosstalk that underlies the continuum from metabolic disruption to obesity and ultimately hepatic cancer.

*Corresponding author: Brian York, Ph.D., Department of Molecular and Cellular Biology, Baylor College of Medicine, One Baylor Plaza, Houston, TX 77030, USA, Phone: 713-798-4178, Fax: 713-790-1275, york@bcm.edu.

†These authors contributed equally.

Competing interests: The authors have declared that no competing interests exist.

Supplementary Information: Supplementary information of this article can be found online at http://www.jbmethods.org/jbm/rt/suppFiles/77.

Keywords

endothelium; hepatocytes; liver cancer; macrophages; obesity

Introduction

The liver coordinately regulates essential aspects of whole-body metabolism, detoxification, and macromolecular synthesis/breakdown. Its architectural infrastructure is composed of small hexagonal lobules, with each lobule connected by a network of sinusoids formed by specialized SEC. In turn, each sinusoid traverses a collection of two primary cell types: hepatocytes (PH), which compose the bulk of liver tissue, and Kupffer cells (MΦ) [1]. Although these cell types demonstrate significant phenotypic and functional heterogeneity, their molecular contributions to metabolic stress and hepatic cancer remain understudied.

Obesity shares aspects of its clinical epidemiology with hepatocellular cancer (HCC), and is considered to be a predisposing risk factor for this type of hepatic cancer [2-4]. Both obesity and HCC are characterized by heightened inflammatory responses that perturb hepatocyte function and promote their transformation [2,4,5]. The presence of tumor myeloid infiltrates is a negative indicator for liver cancer prognosis, as MΦ secrete cytokines that facilitate the inflammatory response and ultimately promote tumor growth [6]. Hypervascularization is a hallmark of HCC, underscoring the role of angiogenesis and altered SEC function during hepatocarcinogenesis [7].

Today's OMICs age of biological and clinical research employs data integration to determine prognostic signatures or identify putative therapeutic targets. Contributions of individual and underrepresented cell types to the molecular signature of a disease are often overlooked, since OMICs datasets are usually obtained from composite samples of the tissue of interest. While a recent study generated proteomic data from individual liver cell types [8], no other study has reported in-depth transcriptomic analyses on individual hepatic cell types with a particular focus on determining cell-specific responses to pathological stimuli such as metabolic and oncogenic stress.

Thus, we developed a molecularly validated, multiple antigen-based method by which $CD95^+$ PH, $F4/80^+CD45^+$ MΦ and vascular endothelial-cadherin $(VE\text{-}cad)^+CD45^-$ SEC can be simultaneously isolated and their transcriptomic signatures compared under physiological versus pathological conditions. Earlier efforts to isolate these 3 cell types generally employed crude enzymatic digestion of the liver, followed by centrifugation to fractionate the resulting cell suspension; however this technique yields impure cell preparations, especially for the parenchymal fraction [9]. Only recently have reports of antigen-based strategies emerged wherein magnetic-activated cell sorting (MACS) for Kupffer cells and liver SEC was used to improve the purity of these cell preparations from the parenchymal cell type [8,10]. One major hindrance in developing an antigen-based strategy for co-isolation of hepatocytes, MΦ and SEC has been the controversial characterization of their cell-specific phenotypes. Our initial assessment of cell surface marker expression by each of these cell types in the murine liver was the foundation of our technique that yields relatively

pure, reproducible, phenotypically- and functionally-defined cell preparations for subsequent downstream analyses.

As proof-of-principle, we utilized this method to qualitatively compare the PH-, MΦ-, and SEC-specific molecular responses to metabolic and oncogenic insults in the liver *in vivo*. We found negligible changes in PH number upon exposure of the liver to either HFD or DEN. However, liver resident MΦ and SEC populations were notably increased in response to both stressors. Transcriptomic analyses identified characteristic gene "signatures" that define each cell type and their distinct tissue-specific biologies under physiological or pathological stress conditions, and also permitted direct comparison of murine-versus-human gene expression data for clinically relevant applications. The ability to isolate relatively pure populations of viable PH, MΦ and SEC provides an indispensable, multidisciplinary tool for assessing their unique functions, molecular properties and behavior within distinct tissue-specific microenvironments. Collectively, these efforts are critical to improve our understanding of the molecular basis for the initiation and progression of metabolic and oncogenic diseases.

Materials and Methods

Animal care

All experiments were performed in accordance with the Animal Care Research Committee at Baylor College of Medicine. All mice were on a pure C57BL6/J background, maintained at 23°C with 12 h light/dark cycle and fed 2920× Teklad Global rodent chow *ad libitum*.

Liver perfusion and separation of parenchymal from non-parenchymal cell fractions

Liver perfusion and cell separation was performed essentially as described in [11], with modifications as outlined in Figure 1B. Livers from adult C57BL/6 (wild type, WT) male mice were first perfused with phosphate-buffered saline (PBS), then with 0.28 mg/ml collagenase IV (Sigma-Aldrich, St. Louis, MO) via retrograde cannulation of the inferior vena cava and egress through the portal vein [12]. The resulting cell suspension was passed through a 70 μm cell strainer, and then centrifuged at 50 × g for 2 min at 4°C. The pellet was resuspended in a 25:12 mixture of Wash/Plating medium (William's Medium E containing 50 IU Penicillin-Streptomycin, 25 mg Glutamine/Gentamycin, 5 mg Insulin-Transferrin-Selenium [ITS], 2 μg Glucagon, 250 μg Amphotericin B, and 10% fetal bovine serum [FBS]), and 100% Percoll (GE Healthcare Life Sciences, Piscataway, NJ) solution, and then centrifuged at 50 × g and 4°C for 10 min. An additional wash step was performed at 50 × g and 4°C for 2 min using Wash/Plating medium to pellet out the parenchymal fraction (Fig. 1B) that is enriched for PH. Supernatant fluid from the first wash step was centrifuged three more times at 50 × g and 4°C for 3 min to eliminate contaminating hepatocytes from non-parenchymal cells that remain in suspension. The non-parenchymal fractions containing SEC and MΦ from up to four mice were pooled and pelleted by centrifugation at 400 × g and 4°C for 10 min.

MACS separation of CD45$^+$ and CD45$^-$ fractions and FACS isolation of hepatic macrophages and sinusoidal endothelial cells

Hepatic non-parenchymal cell pellets were resuspended in 1 × BD Pharm Lyse (BD Biosciences, San Jose, CA) red blood cell lysing solution for 5 min at RT. HBSS/10% FBS was added to the cell suspension, followed by centrifugation at 400 × g and 4°C for 10 min. The resulting cell pellet was resuspended in 90 μl of de-gassed MACS buffer containing PBS, 0.5% BSA, and 2 mM EDTA per 10^7 total cells. Cells were then magnetically labeled with CD45 micro-beads (Miltenyi Biotec Inc., Auburn, CA) per the manufacturer's specifications. Using an appropriate MACS column (Miltenyi Biotec Inc., San Diego, CA) in the magnetic field of a VarioMACS separator (Miltenyi Biotec Inc.), the CD45$^+$ cell fraction (eluate) was physically separated from the CD45$^-$ fraction (flow-through) (Fig. 1B). To ensure depletion of CD45-expressing cells, the CD45$^-$ flow-through was subjected to an additional purification step using a second MACS column. In lieu of an FcR blocking step, 0.5% BSA in the MACS buffer and 10% FBS in the HBSS buffer were used as non-specific blocking agents as previously described (Fig. S1A) [13,14].

CD45$^+$ and CD45$^-$ cell fractions were pelleted via centrifugation at 400 × g and 4°C for 10 min. Cells were resuspended in HBSS/10% FBS to a concentration of 10^8 cells/ml, and subsequently stained with various combinations of the following rat anti-mouse antibody conjugates (Table S1): VE-cad-eFluor 450, CD45-eFluor 780, CD31-APC, Flk1-PE, CD146-FITC, F4/80-PE, CD11b-PE-Cy7, and CD105/Endoglin-PE (1:100; eBioscience, San Diego, CA). Single cell suspensions were washed and resuspended in HBSS/10% FBS with 10 μg/ml propidium iodide (PI; Sigma-Aldrich) for dead cell discrimination, followed by flow cytometry and fluorescence-activated cell sorting (FACS) using a FACSAria (BD Biosciences) cell sorter (Fig. 1B). Contamination of target cell populations by other cell types was also assessed and shown in Figure S1B.

MACS/FACS selection and analysis of CD95$^+$ primary hepatocytes cell surface markers

Enrichment for primary hepatocytes (PH) was performed by re-suspending the liver parenchymal fraction in HBSS/10%FBS at 10^7 cells/ml, followed by incubation with CD95-Biotin conjugate (1:100, eBioscience) for 30 min at 4°C. Excess unbound primary antibody was removed via washing and centrifugation at 400 × g for 10 min at 4°C; the resulting cell pellet was resuspended in 90 μl of de-gassed MACS buffer/10^7 total cells, followed by magnetic labeling with Anti-Biotin micro-beads (Miltenyi Biotec Inc., Auburn, CA) per the manufacturer's specifications. Magnetic separation was performed using an appropriate MACS column in the magnetic field of a VarioMACS separator, with CD95-expressing primary hepatocytes collected as eluate (Fig. 1B). Hepatocytes were assessed for cell surface marker expression by staining with the following rat anti-mouse antibody conjugates (Table S1): CD95-APC, EpCAM/CD326-PE-Cy7, CD45-eFluor 780, and c-Kit-PE (1:100; eBioscience). Single cell suspensions were washed at 50 × g and 4°C for 3 min, and resuspended in HBSS/10% FBS with 10 μg/ml PI, followed by flow cytometry using a FACSAria cell sorter.

High fat diet (HFD) and diethylnitrosamine (DEN) studies

Adult male C57BL/6 mice subjected to 10 weeks of HFD upon weaning were purchased from Jackson Laboratories (Bar Harbor, ME). For DEN studies, 10 male WT mice were injected intraperitoneally with 25 mg/kg DEN (in DMSO) (Sigma) at post-natal day 15. Tumor progression was monitored for 9 months post-injection. Mice were sacrificed, and livers isolated and manually quantified for tumor burden using a standard micrometer. Untreated C57BL/6 male mice age-matched to HFD-treated or DEN-treated mice were sacrificed at the same time, and their livers harvested as described above.

Cell culture

Cell viability was assessed via trypan blue exclusion. PH (10^6 cells) were seeded in 10 cm pre-coated tissue culture plates (BD Primaria™, BD Biosciences) in Wash/Plating Medium as described above, allowed to attach overnight, followed by a medium change 24 h post-seeding. F4/80$^+$ resident MΦ were FACS-sorted directly onto 6-well pre-coated tissue culture plates (50,000 cells/well; BD Primaria™, BD Biosciences) in Dulbecco's Modified Eagle's Medium (DMEM) with 10% FBS. VE-cad$^+$CD45$^-$ SEC were FACS-sorted directly onto fibronectin-coated 48-well tissue culture plates (2,000 cells/well) in Endothelial Cell Growth Medium-2 (EGM-2; Lonza Inc., Allendale, NJ). All cultures were incubated at 37°C with 5% CO_2 and observed daily.

Oil red O

PH in culture were rinsed with PBS and then fixed with 10% neutral buffered formalin for 30 min at RT. After washing twice with deionized water, 60% isopropanol was applied to the fixed cells for 5 min, followed by a freshly prepared working solution of 1.5 mg/ml Oil Red O in isopropanol for 5 min at RT. The stained, fixed cells were then rinsed with tap water until clear, covered with tap water and viewed on a phase contrast microscope.

LPS treatment of macrophages

MΦ isolated from the liver were cultured in DMEM/F12 supplemented with 10% FBS for 2 days. On the third day, medium was refreshed with or without supplementation with 100 ng/ml LPS (Sigma, L2654). Cells were manually scraped and harvested by centrifugation at 1500 rpm for 5 min after 3 h incubation. Cell pellets were washed twice with PBS (Ca^{2+}/Mg^{2+} free) and used directly for RNA isolation.

Methylcellulose hematopoietic colony-forming assay

To assess the hematopoietic potential of hepatic MΦ and SEC, F4/80$^+$ and VE-cad$^+$CD45$^-$ cells were isolated by FACS and sorted directly into 250 μl of MethoCult GF M3434 hematopoietic cell culture medium (StemCell Technologies, Vancouver, BC) in fibronectin-coated 48-well tissue culture plates (BD BioCoat™, BD Biosciences). All cultures were incubated at 37°C with 5% CO_2, and scored for colony formation at days 1, 3, 5, and 7 as previously described [15].

Tube formation assay

Ten microliter of Matrigel basement membrane matrix (BD Biosciences) was applied per inner well of a 15-well Angiogenesis μ-Slide (ibidi, Planegg, Germany), and allowed to polymerize by incubating at 37°C for at least 30 min. SEC were suspended in Endothelial Growth Medium-2 (EGM-2; Lonza, Basel, Switzerland) at a concentration of 1×10^5 cells/ml following isolation by FACS; 50 μl of single-cell suspension was applied per well over polymerized matrix. Cells were then incubated at 37°C for 20 h until slides were viewed under a phase-contrast microscope.

Reverse transcription, qPCR, and gene expression profiling

RNA was isolated from PH, MΦ, and SEC using the Ambion Pure-link RNA Mini Kit (Life Technologies, Carlsbad, CA) according to the manufacturer's protocol. First strand cDNA synthesis was performed using Superscript VILO according to the manufacturer's instructions (Life Technologies, Carlsbad, CA). Real-time quantitative PCR was carried out using TaqMan Universal PCR Reaction Mix (Applied Life Technologies, Carlsbad, CA) with sequence-specific primers and the Mouse Universal Probe Library (Roche Applied Science, Indianapolis, IN). All gene expression assays were performed in triplicate using at least 3 independently isolated RNA samples, and the resulting data normalized to endogenous 18S rRNA expression. Primer sequences are available upon request.

All microarray data (i.e. untreated (UTR), HFD- and DEN-treated PH, MΦ, and SEC) reflect the mean of 3 sets of independent experiments each from a pool of 3–4 mice, respectively. For gene expression profiling, total RNA was extracted and purified with the RNeasy Mini Kit (Qiagen) per the manufacturer's instructions. RNA was reverse transcribed, and microarray hybridization performed using the Illumina Gene Expression MouseWG-6 v2.0 Expression BeadChip Kit at the Laboratory for Translational Genomics at Baylor College of Medicine. Microarray scanned images were imported to Illumina® GenomeStudio for data quality control, and the transcriptome profile data was quartile-normalized by the Bioconductor lumi package [16]. Differences in gene expression among samples were inferred utilizing the Bioconductor limma package [17] ($P < 0.05$) and imposing a fold change exceeding 1.25× using the R statistical system. All microarray data have been uploaded to the Gene Expression Omnibus (GEO) under reference number GSE67225 (http://www.ncbi.nlm.nih.gov/geo/query/acc.cgi?acc=GSE67225).

Tissue preparation for embedding

For OCT embedding, livers were freshly dissected and fixed in 4% paraformaldehyde (PFA) overnight at 4°C. Tissues were washed several times in PBS, cryoprotected by sequential overnight incubation at 4°C in 15% and 30% sucrose solution, embedded in OCT compound (Sakura Finetek USA, Torrance, CA), quick frozen in liquid nitrogen, and sectioned at 5 μm.

For paraffin embedding, freshly dissected livers were fixed in 10% neutral-buffered formalin overnight at 4°C. Tissues were washed in PBS, stored in 70% ethanol at 4°C until embedded in paraffin and sectioned at 5 μm.

Immunohistochemical staining

For fluorescence immunohistochemical staining, OCT-embedded liver sections were blocked for 4–6 h at RT with NDS blocking medium (10% normal donkey serum (NDS)/ 0.5% bovine serum albumin (BSA) in PBS). Sections were washed twice with PBS, and then incubated overnight at 4°C with 1:100 dilutions of primary antibodies (Table S2) in blocking medium. After several PBS washes, sections were incubated for 2–4 h at RT with the appropriate secondary antibodies (Table S2) diluted at 1:500 with blocking medium, and mounted using Vectashield® Mounting Medium (Vector Laboratories, Burlingame, CA) with DAPI as a nuclear counterstain. Images were captured with a Zeiss AxioObserver microscope fitted with an AxioCam MRm camera, using Zeiss AxioVision version 4.8.2.0 software (Carl Zeiss MicroImaging, Thornwood, NY).

For colorimetric immunohistochemical staining, paraffin-embedded liver sections were deparaffinized and rehydrated using standard methods. Antigen retrieval was performed by incubating sections in 1 × Target Retrieval Solution (Dako, Carpinteria, CA) for 10 min at 95°C. Slides were allowed to cool for 10 min at RT, and then washed twice with PBS for 5 min. Several blocking steps were performed by incubating sections in the following solutions: (1) endogenous immunoperoxidase blocking using 3% hydrogen peroxide solution for 10 min at RT, (2) non-specific blocking using NDS blocking media for 1 h at RT, and (3) endogenous biotin blocking using Streptavidin-Biotin Blocking Kit (Vector Laboratories) per the manufacturer's specifications. Tissue sections were then incubated overnight at 4°C with primary antibodies (Table S2) diluted to 1:100 in 0.2 × NDS blocking medium in TBS with 0.1% Tween-20. After several PBS washes, sections were incubated for 1 h at RT with biotinylated species-specific secondary antibodies (Table S2) diluted to 1:1000 in 0.2 × NDS blocking medium. After washing with PBS, sections were again incubated for 30 min at RT with Pierce High Sensitivity Streptavidin-Labeled Horse Radish Peroxidase (Thermo Fisher Scientific Inc., Rockford, IL) diluted at 1:1000 in PBS. Colorimetric detection of bound antigens was performed using ImmPACT DAB detection reagent (Vector Laboratories, Burlingame, CA) per the manufacturer's specifications. Tissue sections were counterstained with hematoxylin, dehydrated and cleared using standard methods, and mounted using VectaMount® permanent mounting media (Vector Laboratories). Images were captured with a Zeiss AxioObserver microscope fitted with an AxioCam ICc3 color camera, using Zeiss AxioVision version 4.8.2.0 software (Carl Zeiss MicroImaging, Thornwood, NY).

For fluorescence immunohistochemistry, deparaffinization, rehydration, and antigen retrieval of paraffin-embedded liver sections were performed as described above. Non-specific blocking of sections was performed using NDS blocking media for 1 h at RT. Tissue sections were then incubated overnight at 4°C with primary antibodies (Table S2) diluted to 1:100 in 0.2 × NDS blocking medium in TBS with 0.1% Tween-20. After several PBS washes, sections were incubated for 1 h at RT with appropriate combinations of the following fluorophore-conjugated secondary antibodies diluted to 1:500 in 0.2 × NDS blocking medium with 0.1% Tween-20: donkey anti-goat-Alexa Fluor 594, donkey anti-mouse-Alexa 594, and donkey anti-rat-Alexa Fluor 488 (BD Biosciences). Tissue sections were stained with DAPI and mounted using VectaStain mounting medium (Vector

Laboratories). Images were captured with a Zeiss AxioObserver microscope fitted with an AxioCam MRm camera, using Zeiss AxioVision version 4.8.2.0 software (Carl Zeiss MicroImaging).

HCC tumor gene signature

We utilized two public HCC datasets [18,19] (GSE14520 and TC-GA-LIHC (http://cancergenome.nih.gov/)) whose gene signatures were partitioned into up- and down-regulated genes.

Obesity signatures

We utilized the following publicly available obesity gene expression datasets Greenawalt *et al.* [20] (GSE24293), Pihlajamäki *et al.* [21] (GSE15653), Ahrens *et al.* [22] (GSE48452), and Keller *et al.* [23] (GSE10785), deposited at Gene Expression Omnibus (GEO) repository (http://www.ncbi.nlm.nih.gov/geo/).

Calculation of gene signature score in obesity and HCC patient cohorts

For each public dataset, we replaced the gene expression of each gene with the z-score with respect to the specimens available in each cohort. For each of the signatures, we computed the sum of z-scores for each sample as described previously [24], adding the z-score for up-regulated genes and subtracting it for down-regulated genes. Finally, for each pair of signatures we plotted the cumulative z-scores on the X- and Y-axes, and computed the Pearson Correlation Coefficient R and associated p-value using the R statistical system and the Python matplotlib library.

Gene set enrichment analysis

Gene Set Enrichment Analysis (GSEA) was carried out using the GSEA pre-ranked tool in the GSEA software package [25] to assess the degree of similarity among the studied gene signatures. After ranking all the genes by fold change, Normalized Enrichment Score (NES) and adjusted q-values were computed utilizing the GSEA method, based on 1000 random permutations. We further determined enriched pathways by employing the gene set collections at the Molecular Signature Database (MSigDB, http://www.broadinstitute.org/gsea/msigdb/) using a hypergeometric distribution ($P < 0.05$).

Results

Antigen-based protocol for simultaneous isolation of hepatocytes, macrophages and SEC

Of the numerous cell types in liver, PH constitute the majority of the parenchymal fraction (PF), whereas liver-specific MΦ, and SEC that line the microvasculature are found in the non-parenchymal fraction (NPF) [1]. Figure 1A [i] shows the cellular architecture of the liver in section with an illustration of the spatial relationships between the liver cell types phenotypically characterized in this study (Fig. 1A [ii]).

We developed an antigen-based protocol for the simultaneous isolation and purification of PH, MΦ and SEC from murine liver with the critical benefit of maintaining cell viability (Fig. 1B). Efficient dissociation of bulk liver is accomplished by collagenase perfusion

through the inferior vena cava and egress through the portal vein, followed by separation of the hepatocyte-containing PF from the NPF by low-speed centrifugation. Isolation of bulk liver tissue is followed by a two-step cellular isolation process, the first involving MACS to separate PH from the PF, and to separate hepatic MΦ ($CD45^+$ fraction) from SEC ($CD45^-$ fraction). The second step utilizes FACS to isolate MΦ from bulk $CD45^+$ fractions based on differential expression of F4/80 by MΦ (Fig. 1B, blue box). Hepatic SEC are isolated from the bulk $CD45^-$ fraction by differential expression of VE-cad (Fig. 1B, red box). Because this isolation strategy relies on the combinations of multiple antigenic markers by each target cell type, it results in high purity cell preparations, and also allows both quantitative and qualitative assessment of each cell type in the liver.

Liver parenchymal fraction is enriched for CD95-expressing hepatocytes

We improved existing PH isolation strategies [26] by MACS of the PF to enrich for PH, which constitutively express low levels of CD95 [27] (Fig. 1B). Approximately 80% of cells in the PF express CD95 as demonstrated by flow cytometry (Fig. 2A). A second population of smaller cells in the PF are $CD95^-$ (Fig. 2A) but were excluded as they fail to meet our criteria for PH. Immunostaining for CD95 verifies its expression in PH (Fig. 2B [i] and Fig. S2C-E). CD95 is co-expressed with canonical intracellular PH markers (i.e. albumin and cytokeratin 8) (Fig. S2C and D). The expression of several cell surface markers associated with murine hepatocytes within the $CD95^+$ fraction of the PF was also assessed via FACS and immunohistochemistry (Fig. S2A and B).

Cultured $CD95^+$ PH displayed morphology of mature hepatocytes, with mono- and bi-nuclear cells present, along with lipid accumulation as confirmed by Oil Red O staining (Fig. 2C [i-ii]). Expression of hepatocyte-associated genes was further assessed via qPCR. Consistent with immunohistological data, expression of mature PH markers *Alb* and *CK8* was enriched in the PH fraction compared to the other two cell fractions, along with other hepatocyte-associated genes (Fig. 2D). These data demonstrate that our improved method for isolation and enrichment of $CD95^+$ cells from the liver PF yields relatively pure cell preparation of functional PH.

$CD45^+$ non-parenchymal fractions are enriched for $F4/80^+$ macrophages

CD45 is generally regarded as a pan-hematopoietic cell marker [28]. We selected three myeloid cell surface antigens, F4/80, CD11b, and CD16/32, which are strongly correlated with tissue-resident MΦ [29], and compared their expression between the $CD45^+$ and $CD45^-$ fractions of the liver NPF. All three markers were highly enriched within the $CD45^+$ fraction (Fig. 3A and B, Fig. S3A).

Immunohistochemical staining revealed cells closely associated with sinusoids and frequently located at bifurcations [1], which strongly express F4/80 (Fig. 3C [i]) and CD45 (Fig. 4C [ii]). Co-localization of F4/80 with CD45 or CD11b is also evident (Fig. 3C [ii-iii], Fig. S3B and C). We therefore define hepatic MΦ as $F4/80^+CD45^+$ non-parenchymal cells.

$F4/80^+CD45^+$ MΦ are small, spherical cells in culture (Fig. 3C [iv]). In methylcellulose, hepatic MΦ displayed *in vitro* hematopoietic colony-forming ability whereas SEC showed

no such activity (Fig. 3D [i]). Moreover, only lineage-restricted granulocyte-macrophage colonies were formed by MΦ in this assay (Fig. 3D [ii]). Thus, not only is hematopoietic colony-forming ability unique to F4/80^{+}CD45^{+} MΦ, but the colony-forming capacity of hepatic MΦ is limited to cells of the granulocyte-myeloid lineage. Expression of MΦ-associated genes was enriched in liver MΦ assessed via qPCR (Fig. 3E). We also examined the effect of LPS on inflammatory gene expression in cultured MΦ and found transcripts encoding pro-inflammatory cytokines significantly up-regulated (Fig. 3F). Thus, hepatic MΦ displayed canonical gene expression and colony-forming activity *in vitro*, demonstrating that our isolation procedure allows antigen-based isolation of relatively pure and functionally responsive hepatic MΦ.

CD45^{-} non-parenchymal fractions are enriched for VE-cad^{+} sinusoidal endothelial cells

We compared expression of endothelial cell markers (VE-cad, CD31, Flk1, CD146, and CD105) between the CD45^{+} and CD45^{-} subsets of the liver NPF (Fig. 4A). Only VE-cad was enriched in the CD45^{-} fraction (Fig. 4A). In contrast, common endothelial markers (i.e. CD31, Flk1, CD105, CD146) were also expressed by cells in the CD45^{+} fraction (Fig. 4A). CD45^{+} cells of hematopoietic origin (i.e. circulating monocytes) can express CD31 and Flk1 [30], while expression of CD146, a marker commonly used to define and isolate liver SEC [8,10] is reported in mesenchymal cells [31]. CD105, on the other hand, is expressed by many hematopoietic cells, including CD45^{-} erythrocytes [32]. Examining various combinations of endothelial markers, we found that only a small fraction of hepatic CD45^{-} cells express SEC markers such as VE-cad, CD31 (Fig. 4B [i]), and Flk1 (Fig. S4A). In contrast, over half of VE-cad^{+} NPF cells co-express CD31 and Flk1, while a smaller fraction of hepatic VE-cad^{+} cells co-express CD146 (Fig. 4B [ii]).

In situ, VE-cad^{+} cells line the hepatic sinusoids and even some larger vessels (Fig. 4C [i]). Such structures lack CD45 expression (Fig. 4C [ii]), consistent with our findings on endothelial cell surface marker expression analyzed by FACS. Co-expression of VE-cad was observed with CD31 (Fig. 4C [iii]; and Fig. S4B) and Flk1 (Fig. S4C). Furthermore, some VE-cad^{+} cells fail to co-express either CD31 (Fig. 4C [iii]) or Flk1 (Fig. S4C), demonstrating correlation of our immunohistochemical characterization with FACS analysis of hepatic SEC phenotypes, which we define as VE-cad^{+}CD45^{-} non-parenchymal cells.

VE-cad^{+}CD45^{-} cells displayed characteristic cobblestone endothelial morphology when cultured on fibronectin (Fig. 4C [iv]). Expression of SEC-associated genes were significantly enriched in SEC but negligibly expressed by PH or MΦ (Fig. 4D). VE-cad^{+}CD45^{-} cells failed to form hematopoietic colonies after 7 days in methylcellulose culture (Fig. 3E), but demonstrated hallmark endothelial cell behavior and function *in vitro*, forming capillary tube networks when seeded in basement membrane matrix (Fig. 4E). Thus, our separation scheme yields highly purified and functional hepatic SEC.

Metabolic and oncogenic stresses increase hepatic MΦ and SEC number

To demonstrate the utility of this co-isolation protocol, we evaluated the effect of pathologic stresses on hepatic cell populations by quantifying the respective frequencies of these cell types in wild type mice fed either a high-fat diet (HFD) for 10 weeks or subjected to

oncogenic stress via exposure to the hepatic-specific chemical carcinogen, diethylnitrosamine (DEN). This approach allowed us to efficiently and simultaneously dissect the relative contribution of each cell type to the resulting phenotype. Whereas HFD and DEN treatment only marginally affected PH number, we observed significant increases in hepatic MΦ and SEC (Fig. 5A and B). Since there was no significant change in the $CD45^+$ or $CD45^-$ populations of the NPF under these pathologic conditions (Fig. S5A and B), these fold-change values accurately reflect numerical changes in MΦ and SEC within the entire liver.

H&E-stained sections of HFD- and DEN-treated livers revealed areas with noticeably increased adipose stores (black arrows), MΦ infiltration (blue box), and increased number and/or caliber of sinusoidal vessels (red arrows) compared to untreated livers (Fig. 5C). Immunohistochemical staining for F4/80 to localize MΦ in both diseased and untreated livers confirmed increased $F4/80^+$ MΦ infiltrates in HFD and DEN livers compared to untreated controls (Fig. 5C, blue arrows). Similarly, $VEcad^+$ SEC (red arrows) lining the hepatic sinusoids showed expansion in both number and caliber in HFD- and DEN-treated livers (Fig. 5C). Immunohistochemical staining for CD95 suggests negligible changes in number of CD95-expressing PH in response to DEN treatment, although there appears to be an increase in the expression of CD95 within hepatic cell types (Fig. 5C).

Metabolic and oncogenic stress induced changes in cell-specific transcriptional fingerprints

Our strategy for co-isolation of three liver cell types provides us with the ability to analyze cell-specific transcriptional changes upon exposure to metabolic or oncogenic stress. We isolated PH, MΦ and SEC from HFD- and DEN-treated mice and their untreated (UTR) counterparts, using the protocol outlined in Figure 1B. RNA was isolated from each cell preparation and assayed by transcriptomic analyses. Hierarchical clustering was applied to compare replicates for each cell type under each treatment group, with each replicate represented by a pool of cells isolated from 3–4 mice. Each of the three liver cell types clustered closely, regardless of treatment (Fig. S5C and D). This initial clustering analysis also revealed cassettes of genes whose expression either increased or decreased in PH, MΦ, and SEC following HFD or DEN treatment (Fig. S5E).

We normalized the HFD and DEN gene expression data relative to the UTR control, and again performed hierarchical clustering to determine gene expression changes that were uniquely and/or commonly induced by either stress to each cell type in the liver (Fig. 5D). In PH and SEC, DEN treatment elicited a greater number of changes in gene expression relative to the UTR control than did HFD, although there were a significant number of genes commonly induced or suppressed by both pathological stresses (Fig. 5D and Fig. S5F and G). On the other hand, the transcriptional responses of MΦ to HFD and DEN were nearly identical and show a significant overlap in their gene expression profiles (Fig. 5D, Fig. S5F and G).

Gene Set Enrichment Analysis (GSEA) was performed to compare the gene signatures of each hepatic cell type to determine how closely each hepatic cell type transcriptionally responds to either metabolic (HFD) or oncogenic stress (DEN) (Fig. 5E). Genes that were

induced in HFD-treated PH displayed positive Normalized Enrichment Scores (NES) when compared to those induced in DEN-treated PH. Conversely, HFD-suppressed PH genes displayed a negative NES when compared to DEN-suppressed PH genes. These findings demonstrate close correlation between the transcriptional responses of PH to metabolic and oncogenic stress. We observed similar trends for correlation of NES scores for hepatic MΦ and SEC exposed to the same challenges (Fig. 5E), suggesting highly convergent transcriptional responses by these key liver cell types when placed under metabolic or oncogenic duress.

Gene ontology (GO) analyses were performed using the gene signatures determined from the HFD- and DEN-treated datasets for PH, MΦ and SEC (Fig. 5F). A considerable number of altered pathways shared between the HFD- and DEN-treated gene signatures were revealed by these analyses. In addition, the robustness of these commonly altered pathways clearly reflects the biology of each cell type analyzed. For example, GO analysis of PH predominantly revealed alterations in metabolic processes, including insulin signaling and diabetes pathways (Fig. 5F) whereas HFD- and DEN-treatment altered cytokine signaling and hematopoietic pathways in MΦ. Finally, liver SEC displayed transcriptional responses in pathways including eNOS activation and regulation as well as tetrahydrobiopterin (BH4) synthesis and regulation, suggesting endothelial cell dysfunction upon exposure to HFD or DEN (Fig. 5F).

HFD-suppressed genes in PH, MΦ and SEC correlate with down-regulated genes from a human obese liver gene set

We also performed GSEA to compare the gene signatures of HFD-treated PH, MΦ, and SEC to a human obese liver gene signature [20] to determine which, if any, of the three liver cell types possess a gene signature that closely recapitulates the gene signature derived from unfractionated human liver biopsies. HFD-suppressed genes in PH and MΦ displayed negative NES when compared to the down-regulated gene signature for a human obese liver dataset (Fig. 6A and B), denoting close correlation. However, HFD-induced genes from all three liver cell types displayed an inverse correlation with the up-regulated human obese liver gene signature (Fig. 6A and B). Since our HFD-treated PH gene signature gave a direct correlation when compared to a murine obese whole liver gene set [23] (Fig. S6A and B), it is unlikely that the negative enrichment scores observed when comparing our murine cell-centric data to human obese gene signatures are the result of experimental or computational artifacts. Instead, these discrepancies likely reflect the inherent variability in human samples as opposed to controlled murine obesity models, and of the broad and ill-defined clinical metrics for diagnosing obesity. In fact, a cross-comparison of three human obesity liver gene signatures [20-22] demonstrated inconsistent correlation of gene expression within these available human datasets (Fig. S6C).

Nevertheless, we performed GO analyses using gene signatures determined from the HFD-treated PH, MΦ, and SEC datasets and the human obese liver gene set [20]. Although only genes down regulated in obesity directly correlated with our HFD gene sets, GSEA (Fig. 6A and B) revealed a significant number of altered pathways shared between our HFD-treated data and the human obese liver gene signatures, including pathways that not only reflect the

biology of the disease (i.e. metabolic and inflammatory pathways), but also the biology of each respective cell type (Fig. 6C and Fig. S9).

Gene expression signature from DEN-treated PH directly correlates with a human HCC gene signature

We performed GSEA to compare the gene signatures of DEN-treated PH, MΦ, and SEC to a publically available human HCC gene signature [18,19]. Of the three liver cell types included in this study, only the PH gene signature identically matched the human HCC gene signature (Fig. 6D and E), consistent with the known pathology of the disease [33,34] and mode of action of the chemical carcinogen DEN [35]. Genes that are induced by DEN treatment in PH are also highly expressed in HCC, whereas DEN-suppressed genes in PH were also down-regulated in the human dataset (Fig. 6D and E). Our DEN-treated liver PH gene signature also directly correlated with the HCC gene profile from Roessler *et al.* [18,19] (Fig. S8C [i], r = 0.59), as well as with a second HCC dataset from TCGA-LIHC (Fig. S8C [ii], r = 0.61). These two human HCC datasets also demonstrate nearly perfect direct correlation when compared with one another (Fig. S8C [iii], r = 0.94).

GO analyses were performed using gene signatures from DEN-treated liver PH, MΦ, and SEC datasets and the human HCC gene set (Fig. 6F, Fig. S8A and B). Similar to previous GO analyses we have performed, we observed perturbations in pathways common to both our mouse datasets and human gene signatures that are characteristic of the disease as well as of each respective cell type.

With the aim of understanding not just how these mouse models for these diseases correlate with their actual human pathologies, but also which transcriptional programs may be initially perturbed and continue to persist from a state of metabolic dysfunction through its progression to liver cancer, we looked at pathways that were perturbed in all HFD- and DEN-treated datasets as well as in the human obese and HCC datasets. From here we gain clues as to how external stimuli, specifically metabolic insults and hepatocarcinogens, could influence transcriptional reprogramming of each of the three liver cell types considered in this study (Fig. 7). This data integration clearly illustrates how information can be extrapolated from each of the cell-specific datasets in order to gain greater insight into the molecular underpinnings for human disease.

In summary, we have developed a highly specific antigen-based cell isolation strategy, and demonstrated its practical application for assessing the fractional cellular response of three hepatic cell types (i.e. PH, MΦ, and SEC) to metabolic and oncogenic stress. On a cellular level, we were able to quantify changes in number, distribution, and localization of each of these cell types in response to HFD or DEN. We were also able to determine the cell-specific and stress-specific transcriptional response to HFD and DEN of each cell type using transcriptomic analyses. Perhaps most importantly, we demonstrate the enormous potential of acquiring cell-specific gene expression data following fractionation of whole tissues, and comparing it to human patient data, to achieve a more nuanced understanding of the pathophysiology and biology of liver disease.

Discussion

We have described an antigen-based isolation procedure that enables the simultaneous recovery of three different hepatic cell types with a high degree of purity. This strategy is indispensable for assessing not only unique and intrinsic cellular properties and functions, but also for elucidating how cell-to-cell interactions influence one another and contribute to whole-organ biology. This approach is particularly important for metabolic tissues like the liver, whose normal activities rely upon functional cooperation among distinct cell lineages. These findings represent a major advance over previous methods of conducting disease-specific gene expression analyses, and eliminates the caveat of relying upon data “averages” yielded by the combined contributions of all cells within a tissue, a situation that both complicates and oversimplifies data interpretation by masking the contributions of minority cell populations.

Accurately determining the tissue-specific cell surface phenotype of each cell type of interest in this study was essential to improve upon existing protocols for isolation of murine hepatic cell types [9,10,36]. For instance, we utilized a surface marker to further enrich for $CD95^{+}$ PH in the parenchymal fraction, in comparison to previous studies that either use the bulk parenchymal fraction as PH [10], or simply use CD95 to assess purity of their hepatocyte preparation [27]. We also define hepatic MΦ and SEC using a combination of surface antigens that permit more specific cell preparations, with MΦ expressing both F4/80 and CD45, and SEC expressing VE-cadherin, but not CD45. Lastly, incorporation of flow cytometric analysis presents another advantage and utility to our approach, because it allows quantitative assessment of absolute cell number and relative frequencies, especially under pathological conditions.

Obesity and chronic liver diseases, including hepatocellular carcinoma, share surprisingly similar epidemiology [4,5], as well as altered gene expression and metabolism in a number of common cell types including PH, MΦ, and SEC. Characterized as a chronic, low-grade inflammatory disease, obesity is a risk factor for HCC as chronic inflammation drives liver cancer progression and metastasis [4,5]. Hepatocytes in a chronic inflammatory environment become more apoptotic, activate tissue-resident MΦ, and recruit other inflammatory cells, which then switch to a pro-inflammatory state. Chemokines secreted by these activated cells act in paracrine and autocrine manners to promote insulin resistance and tumorigenesis [4,5]. Using established experimental mouse models for obesity and liver cancer, we examined PH, MΦ, and SEC in HFD and DEN-treated mice using the isolation procedure detailed in this study, to decipher how these stress conditions influence cellular composition and global gene expression within the liver.

Consistent with previous reports, we observed an increase in hepatic MΦ number in both HFD and DEN-treated states [37-40]. Microarray analyses revealed that overlap of gene expression signatures between the two treatments is considerable, with significant alterations predominantly in inflammatory and stress response pathways. The exact molecular mechanisms underlying the transcriptional changes in MΦ and how they contribute to the cellular phenotype as reflected in our histological analyses represent promising areas for future study.

Endothelial cell dysfunction is a hallmark of metabolic syndrome and chronic liver disease, and is a key driver in their pathogenesis and progression [41,42]. HCC represents one of the most highly vascularized (“angiogenic”) solid tumors [41], and DEN-treated mice display increased liver angiogenesis; as such, strategic targeting of pro-angiogenic factors has become a major focus of solid cancer therapeutics [39,43,44]. From our observations we have determined that there is a marked increase in hepatic VE-cad^{+}CD45^{-} SEC in mice subjected to either HFD or DEN, and histological evidence suggests an expanded but leaky vasculature in the liver. While our GO analyses reveal alterations in angiogenic, eNOS signaling, and regulatory BH4 pathways suggesting endothelial cell dysfunction, the extent to which SEC functionality either responds to or drives these pathological states still remains to be clarified. Together, these data suggest that the molecular etiology of these two disease states not only involves the same cell type responses, but that cell-specific programs activated under excess caloric stress are fundamentally relevant to the cellular response to oncogenic stress.

The importance and utility of the technical advance presented here was demonstrated by interrogating liver cell-specific responses to two closely related pathological insults, HFD and DEN. The power of this technique not only highlights our ability to quantify changes in cell number in the liver and via flow cytometry, but also to collect highly purified, live, intact fractions of each cell type for downstream analyses. Transcriptomic profiling revealed dramatic gene expression changes induced by HFD or DEN that are specific to each cell type in the liver. For instance, liver PH and SEC responded more robustly to DEN than HFD, while hepatic MΦ responded almost identically to both stressors. Such changes in gene expression can only be appreciated by collecting phenotypically defined cell fractions, and would be lost if these analyses were performed using whole, unfractionated tissues.

Perhaps one of the more important contributions of our improved technical approach is that it provides a template for obtaining cell- and tissue-specific gene expression data, which can be used to interrogate gene signatures from known human pathologies. The fact that the murine PH DEN gene signature correlates strongly with the human HCC signature is somewhat expected, considering the known etiology of the disease and the relative abundance of hepatocytes to other contributing lineages [35]. However, this was not the case for the HFD comparison to the human obese dataset. Although the discrepancy may be due in part to differences in diagnostic criteria for staging human obesity versus HCC, it also highlights the fact that our knowledge of the contributions of non-hepatocyte cells to liver disease is significantly lacking, and emphasizes the utility of our fractionation technique to aid in deciphering the specific contribution of minority cell types to the overarching tissue-specific gene signature. HCC diagnosis and staging is most accurately defined via pathological standards that present more reliable criteria [34]. Our comparative analysis of multiple human obesity and HCC datasets reflects this fact, showing poor correlation between available obesity data, yet demonstrating nearly perfect correlation with two public HCC gene signatures (TCGA-LIHC and [18,19]). In all, these comparisons demonstrate the need to determine cell-specific contributions, as opposed to whole-tissue profiling, to better understand the pathobiology of human diseases.

We have made available a tool for future investigators interested in hepatic biology to assess, characterize, and deconvolute PH-, MΦ-, and SEC-specific responses to practically any experimental or physiologic stimulus, administered either *in vivo* or *in vitro*. This study also provides a much needed cell-specific gene expression array resource that can be exploited to understand the mechanisms underlying: (1) the tissue-specific biology of PH, MΦ and SEC; (2) the pathology of obesity and HCC in the context of their respective murine models; and (3) interactions that exist amongst cells within their native or diseased states.

Supplementary Material

Refer to Web version on PubMed Central for supplementary material.

Acknowledgments

Monoclonal antibody against cytokeratin 8 developed by Philippe Brulet and Rolf Kemler was obtained from the Developmental Studies Hybridoma Bank and maintained at The University of Iowa. Support was provided by the Cytometry and Cell Sorting Core at BCM with NIH funding (P30AI036211, P30CA125123, and S10RR024574). This work primarily was supported by NIH grant R01 GM033976-28 to A.R. Means. The authors acknowledge the joint participation by Adrienne Helis Malvin Medical Research Foundation through its direct engagement in the continuous active conduct of medical research in conjunction with Baylor College of Medicine and the “CaMKK2 inhibitors for therapeutic treatment of hepatic cancer” program for partial support of this work.

References

1. Desmet, VJ. Organizational Principles. In: Arias, IM.; Boyer, JL.; Fausto, N.; Jakoby, WB.; Schachter, DA., et al., editors. The Liver: Biology and Pathobiology. Third. New York: Raven Press Ltd; 1994.
2. Sun B, Karin M. Obesity, inflammation, and liver cancer. J Hepatol. 2011; 56:704–713.10.1016/j.jhep.2011.09.020 [PubMed: 22120206]
3. Michelotti GA, Machado MV, Diehl AM. NAFLD, NASH and liver cancer. Nat Rev Gastroenterol Hepatol. 2013; 10:656–665.10.1038/nrgastro.2013.183 [PubMed: 24080776]
4. Rahman R, Hammoud GM, Almashhrawi AA, Ahmed KT, Ibdah JA. Primary hepatocellular carcinoma and metabolic syndrome: An update. World J Gastrointest Oncol. 2013; 5:186–194.10.4251/wjgo.v5.i9.186 [PubMed: 24069511]
5. Starley BQ, Calcagno CJ, Harrison SA. Nonalcoholic fatty liver disease and hepatocellular carcinoma: a weighty connection. Hepatology. 2010; 51:1820–1832.10.1002/hep.23594 [PubMed: 20432259]
6. Lu M, Wu J, He F, Wang X, Li C, et al. Cell expression patterns of CD147 in N-diethylnitrosamine/phenobarbital-induced mouse hepatocellular carcinoma. J Mol Histol. 2014; 46:79–91.10.1007/s10735-014-9602-3 [PubMed: 25447507]
7. Abel T, El Filali E, Waern J, Schneider IC, Yuan Q, et al. Specific gene delivery to liver sinusoidal and artery endothelial cells. Blood. 2013; 122:2030–2038.10.1182/blood-2012-11-468579 [PubMed: 23884859]
8. Azimifar SB, Nagaraj N, Cox J, Mann M. Cell-Type-Resolved Quantitative Proteomics of Murine Liver. Cell Metab. 2014; 20:1076–1087.10.1016/j.cmet.2014.11.002 [PubMed: 25470552]
9. Smedsrød B, Pertoft H. Preparation of pure hepatocytes and reticuloendothelial cells in high yield from a single rat liver by means of Percoll centrifugation and selective adherence. J Leukoc Biol. 1985; 38:213–230. [PubMed: 2993459]
10. Liu W, Hou Y, Chen H, Wei H, Lin W, et al. Sample preparation method for isolation of single-cell types from mouse liver for proteomic studies. Proteomics. 2011; 11:3556–3564.10.1002/pmic.201100157 [PubMed: 21751380]

11. Qiu Q, Hernandez JC, Dean AM, Rao PH, Darlington GJ. CD24-positive cells from normal adult mouse liver are hepatocyte progenitor cells. Stem Cells Dev. 2011; 20:2177–2188.10.1089/scd.2010.0352 [PubMed: 21361791]
12. Klaunig JE, Goldblatt PJ, Hinton DE, Lipsky MM, Chacko J, et al. Mouse liver cell culture. I. Hepatocyte isolation. In Vitro. 1981; 17:913–925. [PubMed: 6273298]
13. Challen GA, Boles N, Lin KK, Goodell MA. Mouse hematopoietic stem cell identification and analysis. Cytometry A. 2009; 75:14–24.10.1002/cyto.a.20674 [PubMed: 19023891]
14. Schiedlmeier B, Kühlcke K, Eckert HG, Baum C, Zeller WJ, et al. Quantitative assessment of retroviral transfer of the human multidrug resistance 1 gene to human mobilized peripheral blood progenitor cells engrafted in nonobese diabetic/severe combined immunodeficient mice. Blood. 2000; 95:1237–1248. [PubMed: 10666196]
15. Marcelo KL, Sills TM, Coskun S, Vasavada H, Sanglikar S. Retinoic Acid Regulation of Hemogenic Endothelial Cell Specification Requires c-Kit, Notch Signaling and p27-mediated Cell Cycle Control. Developmental Cell. 2013; 27:504–515.10.1016/j.devcel.2013.11.004 [PubMed: 24331925]
16. Du P, Kibbe WA, Lin SM. lumi: a pipeline for processing Illumina microarray. Bioinformatics. 2008; 24:1547–1548.10.1093/bioinformatics/btn224 [PubMed: 18467348]
17. Smyth GK. Linear models and empirical bayes methods for assessing differential expression in microarray experiments. Stat Appl Genet Mol Biol. 2004; 310.2202/1544-6115.1027
18. Roessler S, Jia H, Budhu A, Forgues M, Ye Q, et al. A unique metastasis gene signature enables prediction of tumor relapse in early-stage hepatocellular carcinoma patients. Cancer Res. 2010; 70:10202–10212.10.1158/0008-5472.CAN-10-2607 [PubMed: 21159642]
19. Roessler S, Long EL, Budhu A, Chen Y, Zhao X, et al. Integrative genomic identification of genes on 8p associated with hepatocellular carcinoma progression and patient survival. Gastroenterology. 2011; 142:957–966.10.1053/j.gastro.2011.12.039 [PubMed: 22202459]
20. Greenawalt DM, Dobrin R, Chudin E, Hatoum IJ, Suver C, et al. A survey of the genetics of stomach, liver, and adipose gene expression from a morbidly obese cohort. Genome Res. 2011; 21:1008–1016.10.1101/gr.112821.110 [PubMed: 21602305]
21. Pihlajamäki J, Boes T, Kim E, Dearie F, Kim BW, et al. Thyroid hormone-related regulation of gene expression in human fatty liver. J Clin Endocrinol Metab. 2009; 94:3521–3529.10.1210/jc.2009-0212 [PubMed: 19549744]
22. Ahrens M, Ammerpohl O, von Schönfels W, Kolarova J, Bens S, et al. DNA methylation analysis in nonalcoholic fatty liver disease suggests distinct disease-specific and remodeling signatures after bariatric surgery. Cell Metab. 2013; 18:296–302.10.1016/j.cmet.2013.07.004 [PubMed: 23931760]
23. Keller MP, Choi Y, Wang P, Davis DB, Rabaglia ME, et al. A gene expression network model of type 2 diabetes links cell cycle regulation in islets with diabetes susceptibility. Genome Res. 2008; 18:706–716.10.1101/gr.074914.107 [PubMed: 18347327]
24. Taylor BS, Schultz N, Hieronymus H, Gopalan A, Xiao Y, et al. Integrative genomic profiling of human prostate cancer. Cancer Cell. 2010; 18:11–22.10.1016/j.ccr.2010.05.026 [PubMed: 20579941]
25. Subramanian A, Tamayo P, Mootha VK, Mukherjee S, Ebert BL. Gene set enrichment analysis: A knowledge-based approach for interpreting genome-wide expression profiles. Proceedings of the National Academy of Sciences of the United States of America. 2005; 102:15545–15550.10.1073/pnas.0506580102 [PubMed: 16199517]
26. Li WC, Ralphs KL, Tosh D. Isolation and culture of adult mouse hepatocytes. Methods Mol Biol. 2010; 633:185–196.10.1007/978-1-59745-019-5_13 [PubMed: 20204628]
27. Gonçalves LA, Vigário AM, Penha-Gonçalves C. Improved isolation of murine hepatocytes for *in vitro* malaria liver stage studies. Malar J. 2007; 6:169.10.1186/1475-2875-6-169 [PubMed: 18096071]
28. Rhee I, Veillette A. Protein tyrosine phosphatases in lymphocyte activation and autoimmunity. Nat Immunol. 2012; 13:439–447.10.1038/ni.2246 [PubMed: 22513334]
29. Movita D, Kreefft K, Biesta P, van Oudenaren A, Leenen PJM, et al. Kupffer cells express a unique combination of phenotypic and functional characteristics compared with splenic and

peritoneal macrophages. J Leukoc Biol. 2012; 92:723–733.10.1189/jlb.1111566 [PubMed: 22685319]

30. Kim S, Kim J, Papadopoulos J, Wook Kim S, Maya M, et al. Circulating monocytes expressing CD31: implications for acute and chronic angiogenesis. Am J Pathol. 2009; 174:1972–1980.10.2353/ajpath.2009.080819 [PubMed: 19349357]
31. Espagnolle N, Guilloton F, Deschaseaux F, Gadelorge M, Sensébé L, et al. CD146 expression on mesenchymal stem cells is associated with their vascular smooth muscle commitment. J Cell Mol Med. 2013; 18:104–114.10.1111/jcmm.12168 [PubMed: 24188055]
32. Machherndl-Spandl S, Suessner S, Danzer M, Proell J, Gabriel C, et al. Molecular pathways of early CD105-positive erythroid cells as compared with CD34-positive common precursor cells by flow cytometric cell-sorting and gene expression profiling. Blood Cancer J. 2013; 310.1038/bcj.2012.45
33. Rasool M, Rashid S, Arooj M, Ansari SA, Khan KM, et al. New possibilities in hepatocellular carcinoma treatment. Anticancer Res. 2014; 34:1563–1571. [PubMed: 24692683]
34. Marrero JA, Kudo M, Bronowicki J. The challenge of prognosis and staging for hepatocellular carcinoma. Oncologist. 2010; 15(Suppl 4):23–33.10.1634/theoncologist.2010-S4-23 [PubMed: 21115578]
35. Sell S. Cellular origin of hepatocellular carcinomas. Semin Cell Dev Biol. 2002; 13:419–424. [PubMed: 12468242]
36. Smedsrod B, Pertoft H, Eggertsen G, Sundstrom C. Functional and morphological characterization of cultures of Kupffer cells and liver endothelial cells prepared by means of density separation in Percoll, and selective substrate adherence. Cell Tissue Res. 1985; 241:639–649. [PubMed: 2992796]
37. Stefanovic-Racic M, Yang X, Turner MS, Mantell BS, Stolz DB, et al. Dendritic cells promote macrophage infiltration and comprise a substantial proportion of obesity-associated increases in CD11c+ cells in adipose tissue and liver. Diabetes. 2012; 61:2330–2339.10.2337/db11-1523 [PubMed: 22851575]
38. Xu J, Morinaga H, Oh D, Li P, Chen A, et al. GPR105 ablation prevents inflammation and improves insulin sensitivity in mice with diet-induced obesity. J Immunol. 2012; 189:1992–1999.10.4049/jimmunol.1103207 [PubMed: 22778393]
39. Hara M, Kono H, Furuya S, Hirayama K, Tsuchiya M, et al. Macrophage colony-stimulating factor plays a pivotal role in chemically induced hepatocellular carcinoma in mice. Hepatol Res. 2013; 44:798–811.10.1111/hepr.12174 [PubMed: 23710613]
40. Wu J, Li J, Salcedo R, Mivechi NF, Trinchieri G, et al. The proinflammatory myeloid cell receptor TREM-1 controls Kupffer cell activation and development of hepatocellular carcinoma. Cancer Res. 2012; 72:3977–3986.10.1158/0008-5472.CAN-12-0938 [PubMed: 22719066]
41. Coulon S, Heindryckx F, Geerts A, Van Steenkiste C, Colle I, et al. Angiogenesis in chronic liver disease and its complications. Liver Int. 2010; 31:146–162.10.1111/j.1478-3231.2010.02369.x [PubMed: 21073649]
42. Cao Y. Angiogenesis and vascular functions in modulation of obesity, adipose metabolism, and insulin sensitivity. Cell Metab. 2013; 18:478–489.10.1016/j.cmet.2013.08.008 [PubMed: 24035587]
43. Nasr M, Selima E, Hamed O, Kazem A. Targeting different angiogenic pathways with combination of curcumin, leflunomide and perindopril inhibits diethylnitrosamine-induced hepatocellular carcinoma in mice. Eur J Pharmacol. 2013; 723:267–275.10.1016/j.ejphar.2013.11.022 [PubMed: 24291100]
44. Yoshiji H, Kuriyama S, Yoshii J, Ikenaka Y, Noguchi R, et al. Halting the interaction between vascular endothelial growth factor and its receptors attenuates liver carcinogenesis in mice. Hepatology. 2004; 39:1517–1524.10.1002/hep.20218 [PubMed: 15185292]

Abbreviations used

MΦ	macrophage

SEC	sinusoidal endothelial cell
DEN	diethylnitrosamine
HCC	hepatocellular carcinoma
VE-cad	vascular endothelial-cadherin 5
MACS	magnetic-activated cell sorting
PH	primary hepatocytes
hd-qPCR	high density-quantitative polymerase chain reaction
PF	parenchymal fraction
NPF	non-parenchymal fraction
qPCR	quantitative polymerase chain reaction
LPS	lipopolysaccharide
FACS	fluorescence-activated cell sorting
H&E	hematoxylin and eosin
UTR	untreated
GO	gene ontology
GSEA	gene set enrichment analysis
NES	normalized enrichment score

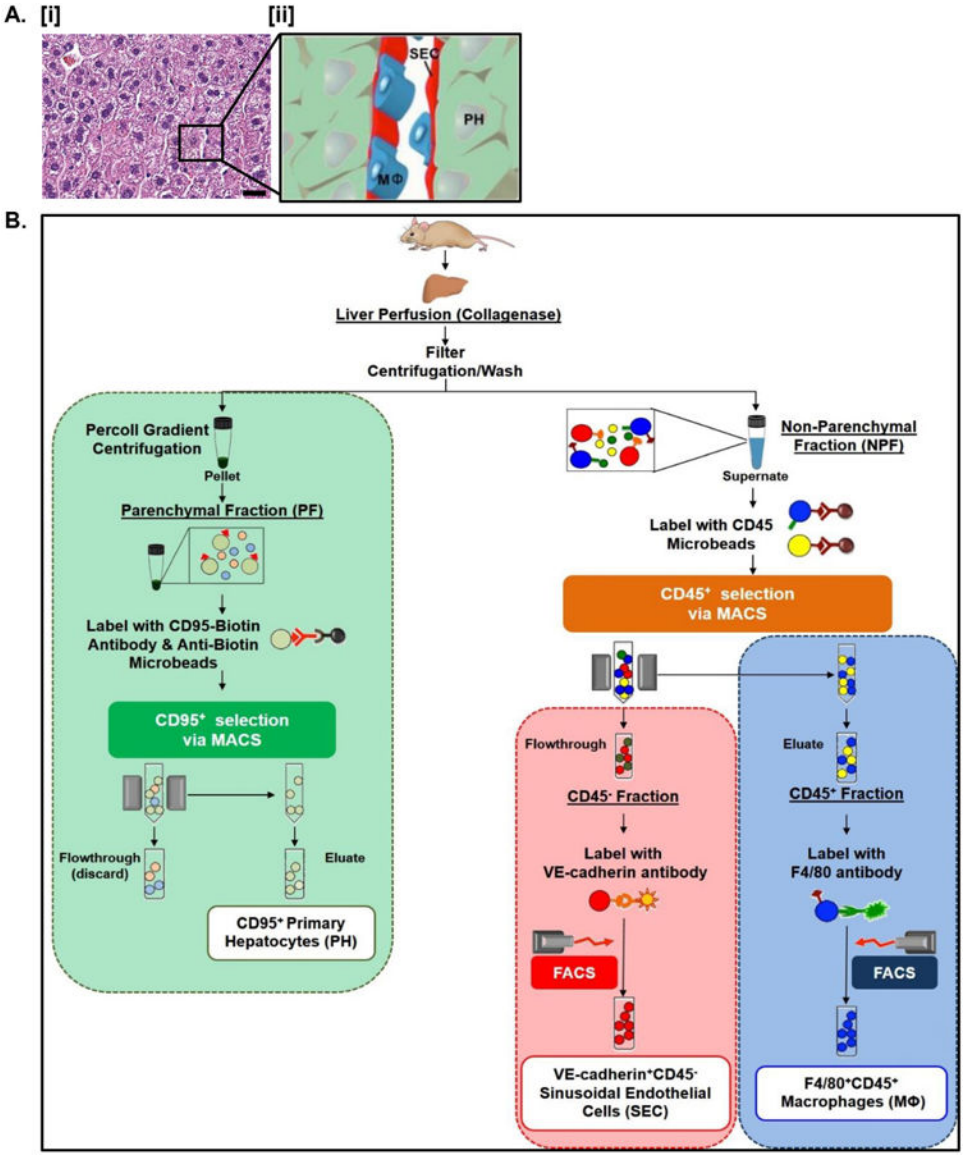

Figure 1. Cell type-specific antigenic marker-based protocol for simultaneous tissue-specific isolation of PH, MΦ, and SEC from murine liver

A. H&E stained paraffin-embedded sections of normal murine liver revealing normal endogenous tissue architecture *in vivo* [i]. The relationship between PH, MΦ, and SEC is highlighted in the accompanying schematic [ii]. Scale bars = 20 μm. See Table S3 for corresponding image magnification. **B.** Flowchart outlining experimental strategy for simultaneous isolation of PH, MΦ, and SEC.

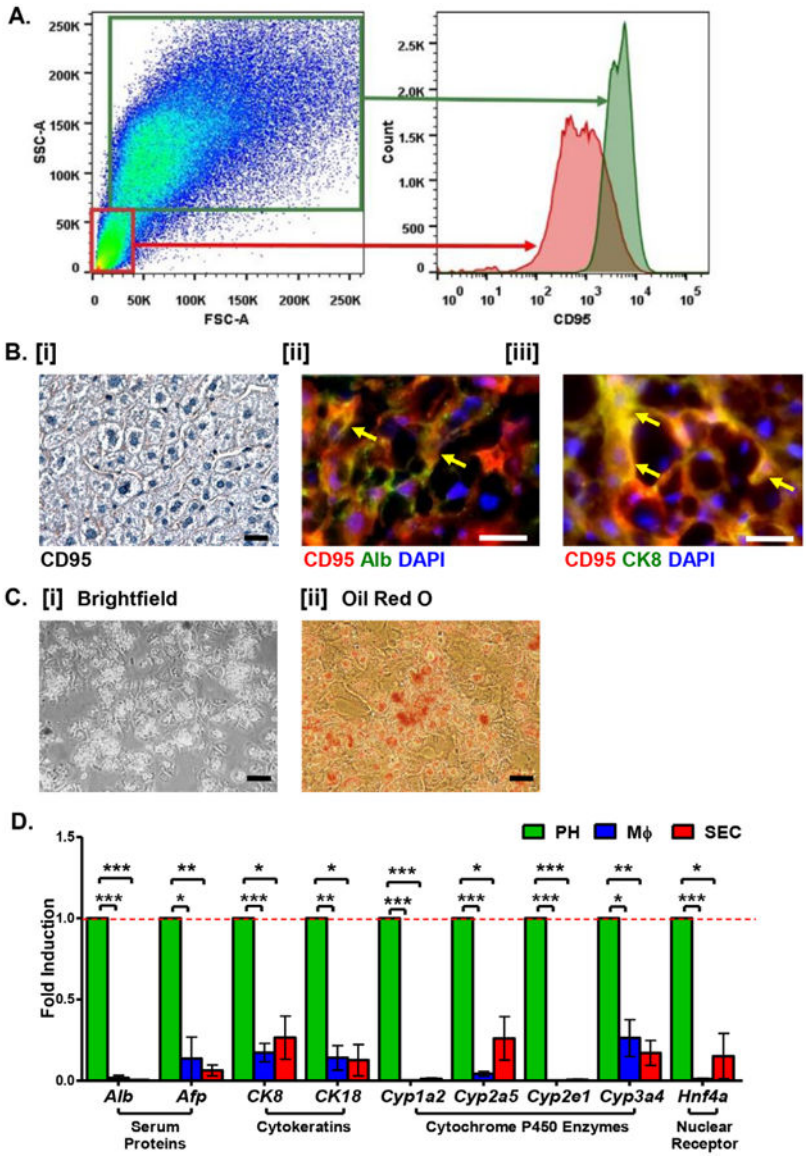

Figure 2. The liver parenchymal fraction is enriched for PH expressing CD95

A. Viable PH are isolated by flow cytometry as CD95+ cells of the liver parenchymal fraction (green box). **B.** [i] Visualization of CD95 expression on murine hepatic cells. [ii] and [iii] Fluorescence immunostaining of normal murine liver reveals co-expression of CD95 (red) with the mature hepatocyte markers Albumin (Alb, [ii]) and cytokeratin 8 (CK8, [iii]). **C.** Culture [i] and Oil Red O [ii] staining of primary isolated CD95+ PH reveals normal morphology and maintenance of neutral lipid synthesis *in vitro*. Scale bars = 20 μm. See Table S3 for corresponding image magnification. **D.** Relative expression (fold induction = 1) of hepatocyte-specific genes in CD95+ PH (green bars) versus MΦ (blue bars) and SEC (red bars) co-isolated from normal murine liver.

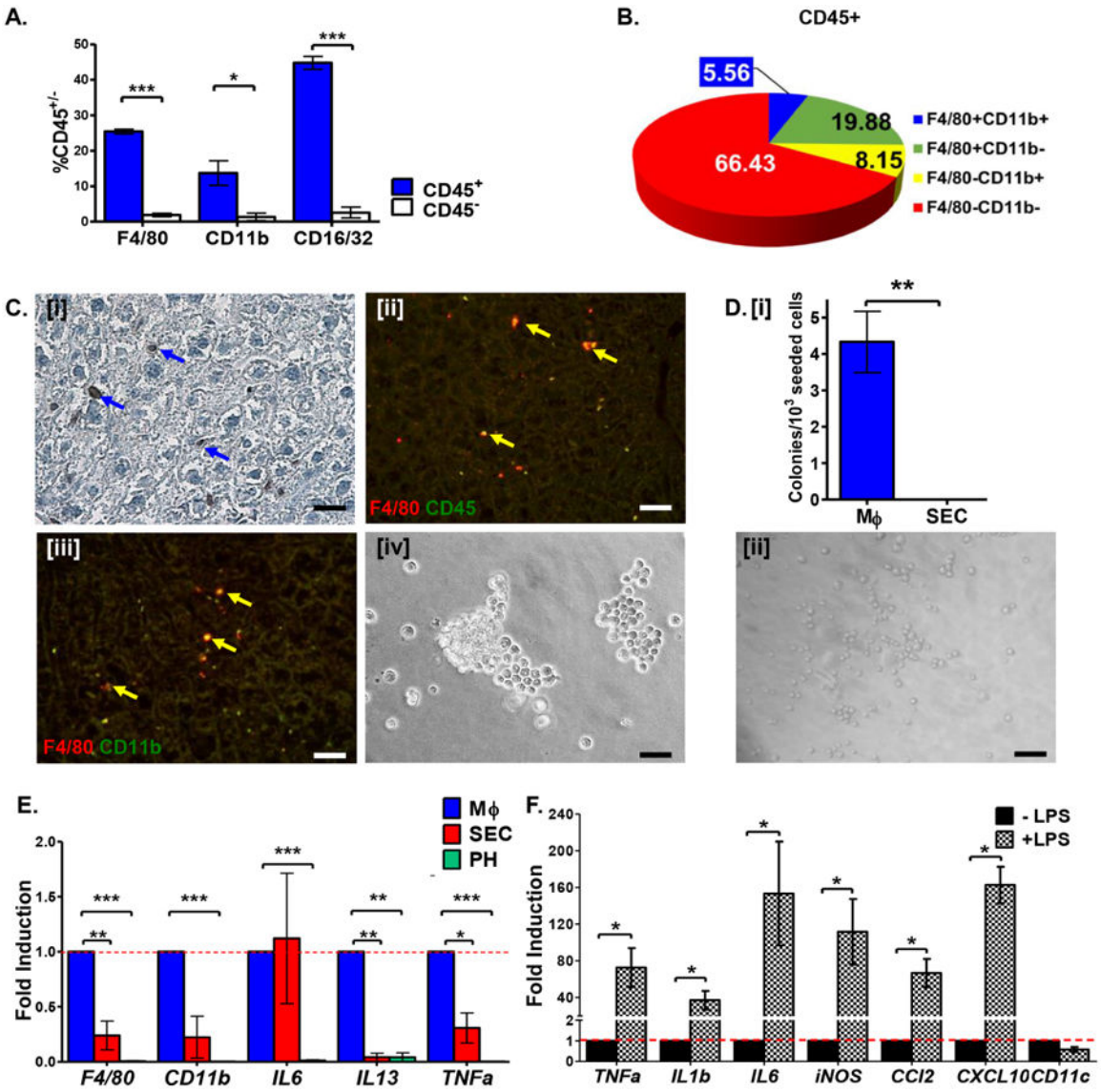

Figure 3. CD45+ cells of the liver NPF are enriched for F4/80+ tissue-resident MΦ

A. Percentage of liver NPF cells expressing characteristic MΦ surface markers within CD45+ and CD45- fractions. **B.** Distribution of characteristic MΦ surface marker expression on CD45+ cells isolated from NPF. **C.** Immunostaining of murine liver sections demonstrating the expression pattern of F4/80 [i] and its co-expression with CD45 [ii] and CD11b [iii]. Isolated F4/80+CD45+ cells exhibit characteristic MΦ morphology *in vitro* [iv]. Scale bars = 20 μm. See Table S3 for corresponding image magnification. **D.** [i] *In vitro* hematopoietic colony-forming potential is restricted to isolated liver F4/80+CD45+ cells seeded into methylcellulose medium on fibronectin-coated plates. [ii] Isolated tissue-specific F4/80+CD45+ cells from liver NPF formed granulocyte-macrophage colony forming units (CFU-GM) in methylcellulose medium. Scale bars = 20 μm. See Table S3 for corresponding image magnification. **E.** Relative expression (fold induction = 1) of MΦ-associated genes is enriched in F4/80+CD45+ cells (blue bars) versus PH (green bars) and SEC (red bars) co-

isolated from normal murine liver. **F.** F4/80+CD45+ MΦ up-regulate transcription of inflammatory cytokines upon stimulation with LPS.

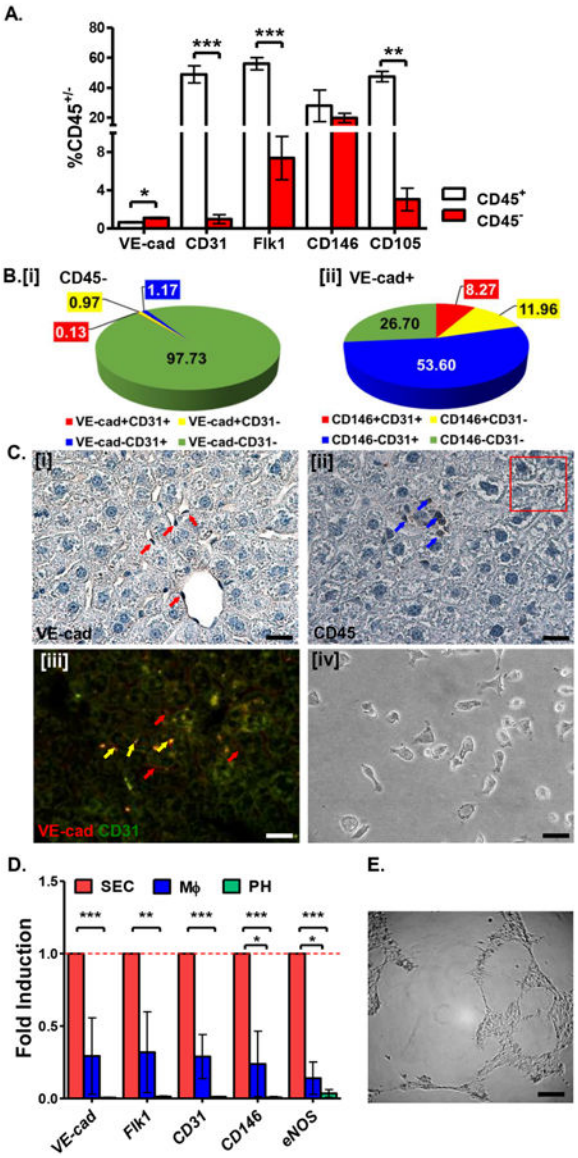

Figure 4. CD45- cells of the liver NPF are enriched for VE-cad+ SEC

A. Percentage of liver NPF cells expressing SEC surface markers within the CD45+ and CD45- fractions. **B.** Distribution of SEC surface marker expression on CD45- cells from liver NPF. **C.** Immunostaining of murine liver sections demonstrates that cells lining the sinusoids express VE-cad [i] but not CD45 [ii]. VE-cad+ cells also co-express CD31 [iii]. Isolated tissue-specific VE-cad+CD45- cells demonstrate characteristic endothelial cell morphology *in vitro* [iv]. Scale bars = 20 μm. See Table S3 for corresponding image magnification. **D.** Relative expression (fold induction=1) of SEC-associated genes is enriched in VE-cad+CD45- cells (red bars) versus PH (green bars) and MΦ (blue bars) co-isolated from normal murine liver. **E.** VE-cad+CD45- SEC exhibits capillary tube-forming activity *in vitro*. Scale bar = 200 μm. See Table S3 for corresponding image magnification.

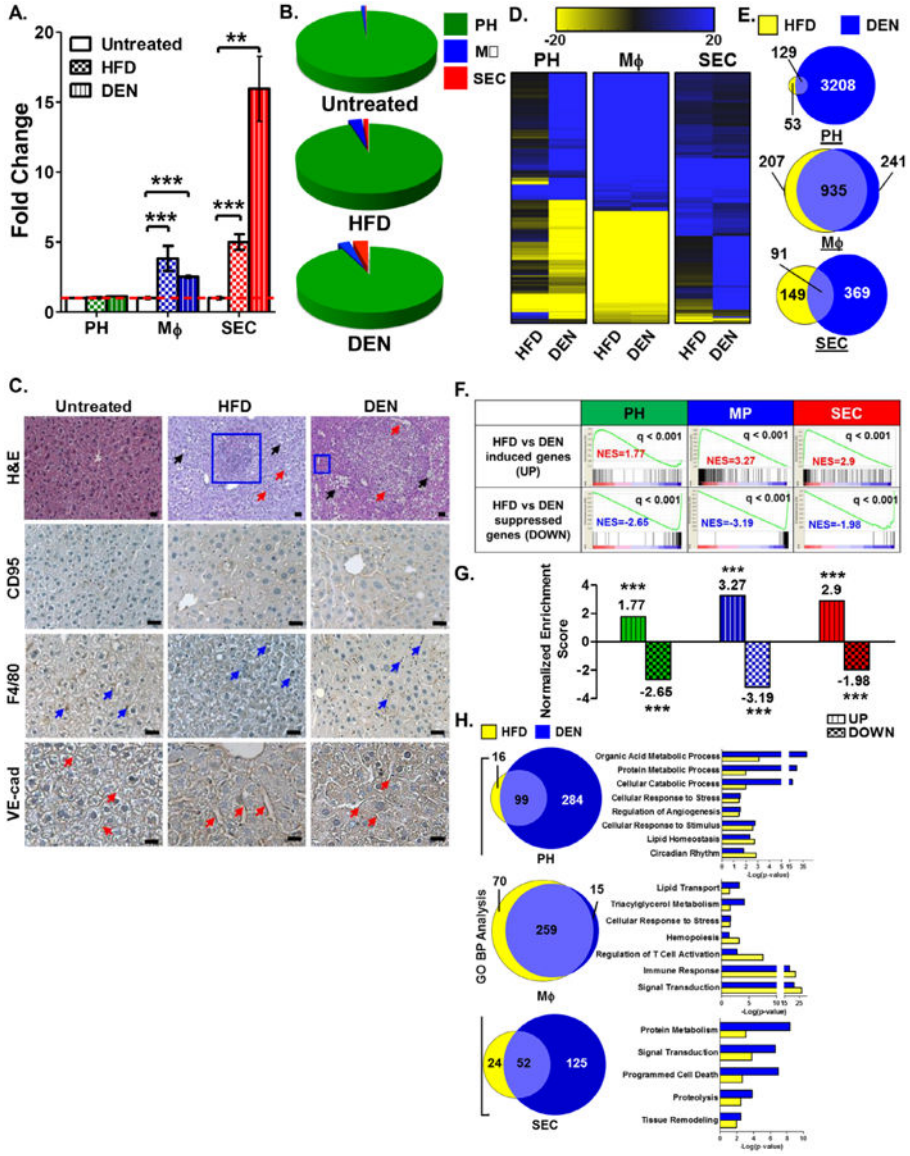

Figure 5. Metabolic and oncogenic stresses increase liver MΦ and SEC numbers

A. Frequency of CD95+ PH within the total PF, hepatic F4/80+ MΦ within the CD45+ fraction, and VE-cad+ SEC within the CD45- fraction from HFD- and DEN-treated WT mice quantified as fold change relative to that observed in an untreated control group (fold change = 1). **B.** Relative proportions of PH, MΦ, and SEC in untreated, HFD- and DEN-treated livers. **C.** H&E staining and immunohistochemical staining for CD95, F4/80 and VE-cad of liver sections from untreated, HFD- and DEN-treated WT mice. Scale bars = 20 μm. See Table S3 for corresponding image magnification. **D.** Comparative global gene expression patterns in PH, MΦ, and SEC co-isolated from HFD- and DEN-treated mice normalized to untreated cell fractions. **E.** Commonality of gene expression changes observed between PH, MΦ, and SEC isolated from HFD- and DEN-treated murine liver relative to untreated (UTR). **F.** Association of gene expression signatures of HFD-treated liver PH, MP, and SEC with gene signature derived from their corresponding DEN-treated liver cell

types. Gene signatures for all three HFD-treated liver cell types matched their corresponding DEN-treated gene signatures. **G.** Normalized enrichment scores (NES) of HFD-induced genes relative to DEN-induced genes (UP) and HFD-suppressed genes relative to DEN-suppressed genes (DOWN) from liver PH, MΦ, and SEC determined via the GSEA method. **H.** Commonality of altered pathways determined via Gene Ontology-Biological Pathways functional analyses observed between HFD- and DEN-treated PH, MΦ, or SEC. Data show the mean of 2 independent samples of a pool of 3–4 animals.

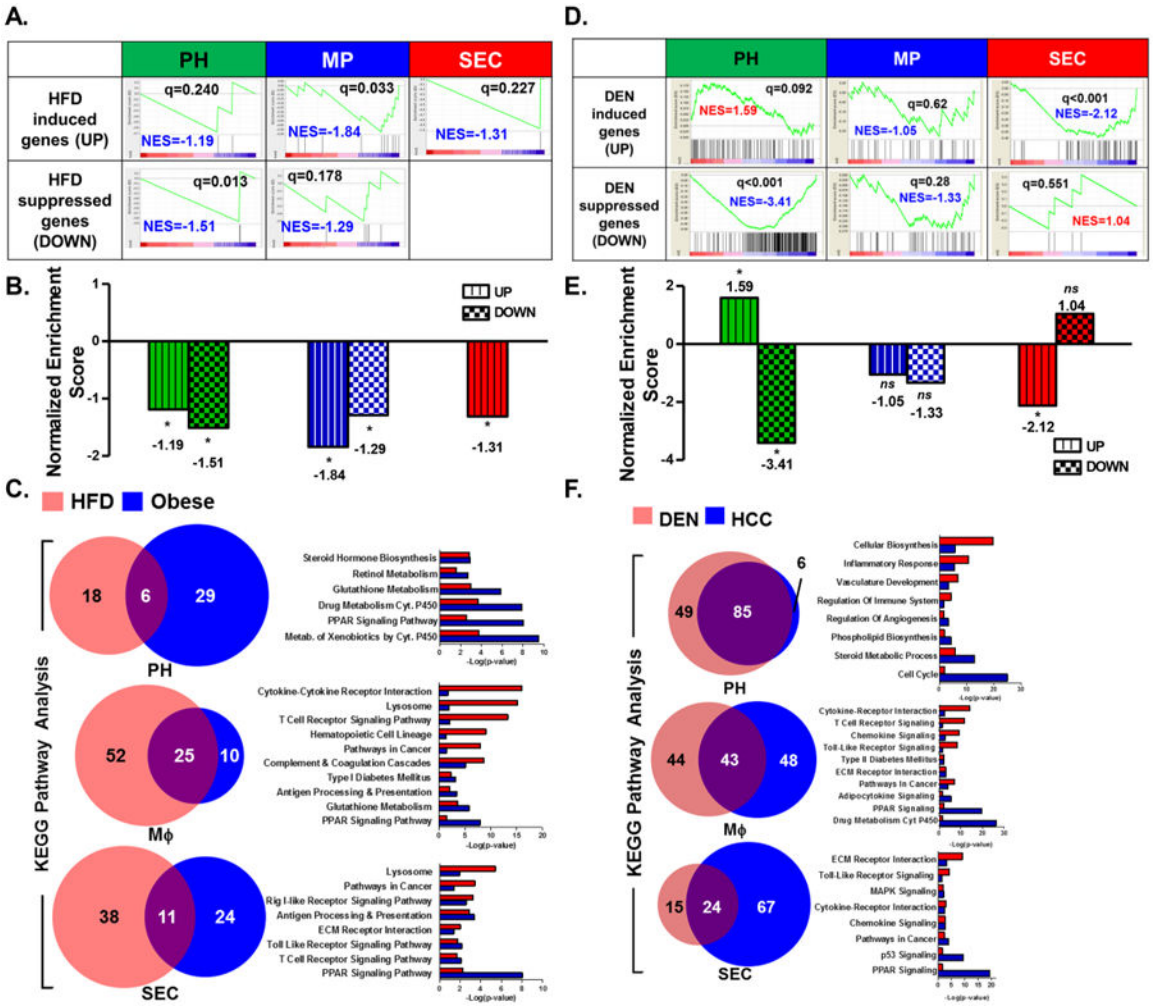

Figure 6. Gene expression signature from DEN-treated PH matched the gene signature from a human HCC gene set

A. Association of gene expression signatures of HFD-treated liver PH, MP, and SEC with gene signature derived from human obese liver biopsies. In all three cell types, only the HFD-suppressed gene signatures matched the human obese liver signature [20]. **B.** Normalized enrichment scores (NES) of HFD-induced (UP) and HFD-suppressed (DOWN) genes from liver PH, MΦ, and SEC relative to a human obese liver gene signature [20] via the GSEA method. **C.** Commonality of altered pathways determined via KEGG Pathway functional analyses observed between HFD-treated PH, MΦ, or SEC and human obese liver gene set [20]. **D.** Association of gene expression signatures of DEN-treated liver PH, MΦ, and SEC with gene signature derived from human HCC tumors [18,19]. Of all three cell types, only PH demonstrated a gene expression signature (both upregulated and down-regulated) that matched the human HCC signature. **E.** Normalized enrichment scores (NES) of DEN-induced (UP) and DEN-suppressed (DOWN) genes from liver PH, MΦ, and SEC relative to the human HCC gene signature [18,19] via the GSEA method. **F.** Commonality of altered pathways determined via KEGG Pathway functional analyses observed between DEN-treated PH, MΦ, or SEC and a human HCC gene set [18,19]. Data show the mean of 2 independent samples of a pool of 3–4 animals.

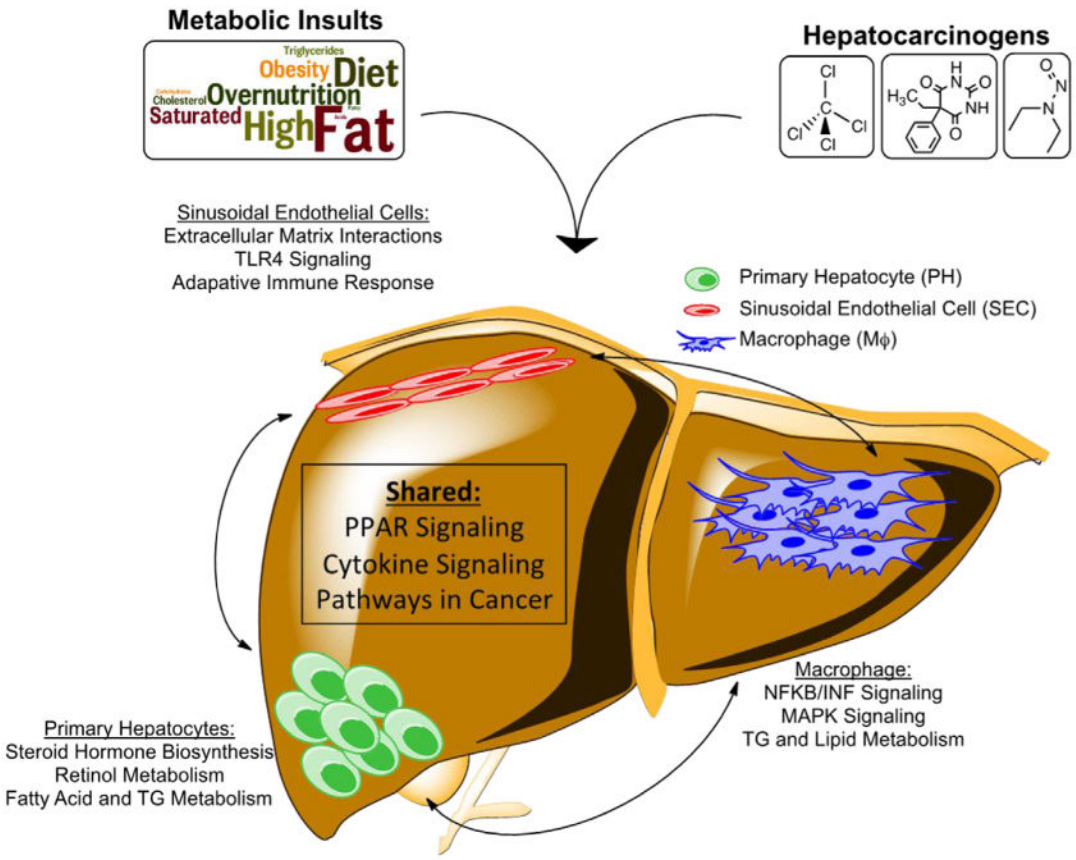

Figure 7. Model of crosstalk among pathways and hepatic cell types in response to metabolic and oncogenic insult

Some pathways are predicted to be altered in all 3 cell types. A number of pathways were only altered specifically in PH, MΦ or SEC.